

Jupiter's Whistler-mode Belts and Electron Slot Region

Y.-X. Hao^{1,2}, Y. Y. Shprits^{1,3,4}, J. D. Menietti⁵, Z. Y. Liu⁶, T. Averkamp⁵,
D. D. Wang¹, P. Kollmann⁷, G. B. Hospodarsky⁵, A. Drozdov⁴, E. Roussos²,
N. Krupp², R. B. Horne⁸, E. E. Woodfield⁸ and S. J. Bolton⁹

Y.-X. Hao, GFZ German Research Centre for Geosciences, 14473 Potsdam, Germany;
Now at Max Planck Institute for Solar System Research, 37077, Germany.
(hao@mps.mpg.de)

¹GFZ German Research Centre for
Geosciences, 14473, Potsdam, Germany

²Max Planck Institute for Solar System
Research, 37077, Goettingen, Germany

³Institute of Physics and Astrophysics,
University of Potsdam, Germany

⁴University of California Los Angeles, Los
Angeles, CA, USA

⁵Department of Physics and Astronomy,
University of Iowa, Iowa City

The spatial distribution of whistler-mode wave emissions in the Jovian magnetosphere measured during the first 45 perijove orbits of Juno is investigated. A double-belt structure in whistler-mode wave intensity is revealed. Between the two whistler-mode belts, there exists a region devoid of 100s keV electrons near the magnetic equator at $9 < M < 16$. Insufficient source electron population in such an electron “slot” region is a possible explanation for the relatively lower wave activity compared to the whistler-mode belts. The wave intensity of the outer whistler-mode belt measured in the dusk-premidnight sector is significantly stronger than in the postmidnight-dawn sector. We suggest that the inherent dawn-dusk asymmetries in source electron distribution and/or auroral hiss emission rather than the modulation

⁶IRAP, CNRS-Universite Toulouse III

Paul Sabatier, Toulouse, France

⁷Johns Hopkins University Applied

Physics Laboratory, Laurel, MD, USA

⁸British Antarctic Survey, High Cross,

Madingley Road, Cambridge, UK

⁹Space Science and Engineering Division,

Southwest Research Institute, San Antonio,

TX, USA

of solar cycle are more likely to result in the azimuthal variation of outer whistler-mode belt intensity during the first 45 Juno perijove orbits.

1. Introduction

1 As the magnetosphere with the most intense radiation belt(s) [e.g., *Mauk and Fox,*
2 2010] in our solar system, the Jovian magnetosphere is an attractive natural laboratory
3 for studying wave-particle interactions. Plasma waves with frequency ranging from below
4 the ion cyclotron frequency (e.g., Alfvén waves [*Saur et al., 2018*]) to above the electron
5 cyclotron frequency (e.g., Z-mode waves [*Menietti et al., 2023b*]) contribute considerably
6 to the dynamics of Jovian energetic electrons. Whistler-mode chorus and hiss waves,
7 which have been demonstrated as key components to the terrestrial electron belt dynamics
8 [*Horne et al., 2005; Allison et al., 2021; Li et al., 2015; Zhao et al., 2019*], are also key
9 drivers of acceleration and loss of energetic electrons trapped in Jupiter’s magnetic field
10 [*Horne et al., 2008; Shprits et al., 2012; Woodfield et al., 2014*].

11 Whistler-mode waves can drive both electron acceleration and loss. The quantifica-
12 tion of their spatial and spectral distributions is necessary for evaluating their impact
13 at Jupiter. A subset of measurements based on Galileo and Juno mission data [*Meni-*
14 *etti et al., 2012, 2021a, b; Li et al., 2020*] have been analyzed. With the Juno Extended
15 Mission updated to the 45th perijove orbits (PJ45) [e.g., *Menietti et al., 2023a*], a larger
16 section of the nightside Jovian magnetosphere within $25R_J$ (R_J denotes Jupiter radius)
17 has been sampled, giving us the opportunity to build a more comprehensive global map
18 of whistle-mode waves.

19 In this study, we focus on the spatial distribution of whistler-mode waves and their
20 links to 30-800 keV electron spectra within $25R_J$, as measured by Juno during its first
21 45 perijove orbits. Unless otherwise stated, the wave frequency range is restricted to be-

22 tween $0.1f_{ceq}$ and $0.8f_{ceq}$ (f_{ceq} denotes the frequency of the equatorial electron cyclotron),
 23 whereas mapped energetic electron fluxes are selected within 4° of magnetic latitude. With
 24 the given frequency range we highlight the spatial distribution of whistler-mode chorus
 25 waves, even if the contribution of auroral hiss waves can not be fully excluded. Cor-
 26 responding energetic electron measurements near the magnetic equator, where whistler-
 27 mode chorus waves are believed to be excited, are also analyzed for context.

2. Banded Chorus Waves Observed at the Magnetic Equator

28 Figure 1 shows an example of whistler-mode chorus emission measured by the Juno
 29 spacecraft near Jupiter's magnetic equator. The top/middle panel displays the elec-
 30 tric/magnetic spectral density detected by the Juno Waves instrument [*Kurth et al.*, 2017]
 31 while the bottom panel shows their ratio E/cB . The harmonic structure above the local
 32 electron cyclotron frequency f_{ce} (calculated with local Juno magnetometer measurements
 33 [*Connerney et al.*, 2017]) was observed between $\sim 16:00-16:15$, during a magnetic equator
 34 crossing. Large E/cB values indicate waves of an electrostatic nature. We note that
 35 such equatorial electrostatic waves with harmonic structure are tell-tale signatures of the
 36 electron cyclotron harmonics (ECH) emissions confined inside the plasma sheet of Jupiter
 37 [c.f., *Menietti et al.*, 2012, Figure 4].

38 In addition to ECH emissions above f_{ce} , emissions between $0.1f_{ce}$ and $0.8f_{ce}$ are also
 39 recorded in Figure 1. Calculated $E/cB < 1$ indicates a clear electromagnetic nature of
 40 these waves. At 15:45-15:55, the emission was confined between $0.1f_{ce}$ and $0.5f_{ce}$, is iden-
 41 tified as typical lower band chorus waves. At 16:00-16:26, wave emissions were observed
 42 in both the $0.1f_{ce} - 0.5f_{ce}$ and $0.5f_{ce} - 1.0f_{ce}$ bands. Burst mode data of the Juno Waves

43 instrument indicate that there existed a distinct power gap between the two frequency
 44 bands below and above $0.5f_{ce}$. Waves with such dual-band structure are reminiscent of
 45 whistler-mode chorus waves in the terrestrial magnetosphere [e.g., *Tsurutani and Smith,*
 46 *1974; Teng et al., 2019*].

3. Global Morphology of Whistler-mode Waves

47 Previous Juno-based studies [*Li et al., 2020; Menietti et al., 2021a, b, 2023a*] presented
 48 the spatial distribution of whistler-mode waves integrated power using f_{lh} or f_{ci} as the
 49 lower cutoff frequency (f_{lhr} : lower hybrid resonance, f_{ci} ion cyclotron frequency). We
 50 note that in these studies, wave intensities between the lower cutoff and $0.1f_{ce}$, which
 51 are likely to be (auroral) hiss waves, are much stronger than the wave intensities above
 52 $0.1f_{ce}$ [e.g, *Li et al., 2020, Figure 4*] and [*Menietti et al., 2021b, Figure 5*]. Therefore,
 53 the global distributions of the integrated whistler-mode wave intensity in *Li et al. [2020]*
 54 and *Menietti et al. [2021b]* mostly depict the wave morphology below $0.1f_{ce}$. As discussed
 55 in Section 2, Juno measurements demonstrate two points that we adopt in the upcoming
 56 sections: 1. Whistler-mode chorus waves in the Jovian magnetosphere show a distinct
 57 frequency band structure similar to the terrestrial chorus waves [*Burtis and Helliwell,*
 58 *1969*]; 2. The electron cyclotron frequency (f_{ceq}) could be a suitable normalization factor
 59 for the spectrum of Jovian chorus waves [*Menietti et al., 2021a, b*], as done for terrestrial
 60 chorus waves [e.g., *Wang et al., 2019*].

61 We focus on the spatial distribution of whistler-mode waves with the frequency range
 62 $0.1-0.8f_{ceq}$, which is in the frequency range of “typical chorus waves” [e.g., *Tsurutani and*
 63 *Smith, 1977; Meredith et al., 2012; Wang et al., 2019*]. We follow the same methodology as

64 for the whistler-mode survey as in *Menietti et al.* [2021a] with data up to PJ45 [*Menietti*
65 *et al.*, 2023a]. The same spatial grid size is adopted ($\Delta M = 1.0$, $\Delta MLT = 1h$, $\Delta \lambda = 2^\circ$
66 for $|\lambda| < 16^\circ$ and $\lambda = 5^\circ$ for $|\lambda| > 16^\circ$, where M, MLT and λ denote the M shell,
67 magnetic local time, and magnetic latitude, respectively) for spatial binning. The M-shell
68 and f_{ceq} are based on the JRM09 plus current sheet model [*Connerney et al.*, 1981, 2018].
69 Spatial grids and the accumulative sampling time of Juno per bin are shown in supporting
70 Figure S1. In this study, the outermost M-shell extends to 25, while the absolute value
71 of magnetic latitude to 36° . Higher latitudes are excluded to minimize the influence of
72 auroral hiss [e.g., Figure 4 of *Li et al.*, 2020]. In terms of MLT, the whole night sector of
73 Jupiter is covered.

74 The integrated wave intensity $\langle B_W^2 \rangle$ in each step of spacecraft sampling (hereafter re-
75 ferred to as “data point”) is the average value of the wave intensity measured over the
76 time interval $\Delta\tau = 1 \text{ min}$. $\langle B_W^2 \rangle$ is calculated with

$$\langle B_W^2 \rangle = \left\langle \int_{uc}^{lc} PSD(f) df \right\rangle, \quad (1)$$

77 between $0.1f_{ceq}$ and $0.8f_{ceq}$ and $PSD(f)$ is the magnetic power spectral density. The
78 frequency-resolved wave intensity $\langle B_{Wi}^2 \rangle$ is calculated within 7 normalized frequency ($\beta =$
79 f/f_{ceq}) bins using:

$$\langle B_{Wi}^2 \rangle = \left\langle \int_{\beta_i - \frac{1}{2}\Delta\beta}^{\beta_i + \frac{1}{2}\Delta\beta} PSD(f_{ceq}\beta) f_{ceq} d\beta \right\rangle, \quad (2)$$

80 in which each bin centers from $\beta_0 = 0.15$ to $\beta_7 = 0.75$ with the bandwidth $\Delta\beta=0.1$.

81 Figure 2 presents the spatial distribution of the average integrated magnetic intensity for
82 whistler-mode waves in the chorus frequency range. Surprisingly, the spatial distribution

83 of whistler-mode wave intensity in typical chorus frequency range exhibits a double-belt
 84 structure. In addition to the intense whistler-mode emission at $5 < M < 9$, another
 85 “whistler-mode belt” emerges at $18 < M < 25$, peaking at $M \approx 21$. The outer whistler-
 86 mode belt is of the strongest intensity around dusk, indicating a possible dawn-dusk
 87 asymmetry of the wave emission. Panels (b) and (c) show the intensity of whistler-mode
 88 emission in the meridian plane, averaged over midnight to dawn and dusk to midnight,
 89 respectively. The outer whistler-mode belt is distinct in both sectors and extends at least
 90 up to $|\lambda| = 21^\circ$. The outer belt whistler-mode wave intensity at the dusk-midnight sector
 91 is stronger in each corresponding $(M, |\lambda|)$ bin, suggesting that the observed dawn-dusk
 92 asymmetry is not due to an orbital bias.

3.1. Double-Belt Structure of Whistler-mode Wave Intensity

93 In Figure 3 we present the median, upper, and lower quartile of whistler-mode wave
 94 intensity as a function of M-shell. Since intense whistler-mode wave emissions have been
 95 reported during Ganymede and Europa flybys [*Gurnett et al.*, 1996; *Shprits et al.*, 2018;
 96 *Kurth et al.*, 2022], possible Galilean-moon flybys have been excluded from our analysis.

97 As shown in Figure 3(a), the median wave intensity of whistler-mode wave exhibits a
 98 distinct double-peaked distribution along the M-shell. The median value of integrated
 99 wave intensity at the belt peaks is comparable ($2 \times 10^{-5} nT^2 \sim 3 \times 10^{-5} nT^2$). The “slot
 100 region” in between the two belts lies roughly between $M = 9$ and 16 with an intensity
 101 minimum of one order of magnitude lower than at the peaks, located at $M \approx 11$. We
 102 further note that within the entire M-shell range, the highest contribution of the integrated

103 intensity comes for the $0.1f_{ceq} - 0.2f_{ceq}$ range. This statistical wave frequency spectrum
 104 is consistent with previous studies [c.f., Figure 5(b) of *Menietti et al.*, 2021b].

105 To explore the possible mechanisms behind the dual whistler belt structure, we in-
 106 vestigate the distribution of energetic electrons measured by Jupiter Energetic-particle
 107 Detector Instrument (Juno/JEDI)[*Mauk et al.*, 2017], using publicly available data up
 108 to PJ44. As various studies [e.g., *Burton and Holzer*, 1974; *Tsurutani and Smith*, 1977;
 109 *Lauben et al.*, 2002] have shown, whistler-mode chorus waves at Earth are excited near the
 110 magnetic equator, therefore we focus on electrons populations measured within 4° of mag-
 111 netic latitude. JEDI measurements during time intervals with “high resolution” spectra
 112 have been interpolated into the “low resolution” energy bins, assuming local power-law
 113 spectra between adjacent energy channels. Figure 3(b) presents the median-averaged
 114 distribution of omni-directional differential fluxes for 30-800 keV electrons within $M=25$.

115 We note that there exists a slot-like region of energetic electrons between $9 < M < 16$,
 116 where a flux depletion of 100s keV electrons by over 2 orders of magnitude is identified.
 117 Such energy-dependent depletion was also seen partially in previous studies [e.g., *Wang*
 118 *et al.*, 2021, Figure 4]. In Figure S2, we present both the median and mean values of
 119 the electron fluxes as a function of the M-shell measured during the first 29 (interval
 120 studied by [*Ma et al.*, 2021]) and 44 orbits (this study) of Juno. We note that due to
 121 the ascending perijove latitude of Juno, orbits PJ01-PJ29 did not cover the near-equator
 122 region at $M < 9$ and conclude that the slot’s appearance is not an averaging method or
 123 data sampling artefact. Most notable, the energetic electron slot coincides with the one
 124 of Jovian whistler-mode waves.

125 We calculate the characteristic energy E_C and total energy flux ϵ_T of the energetic
 126 electrons [Mauk *et al.*, 2004]. As shown in Figure 3(c), characteristic energy of the electron
 127 energy spectra drops steeply down to $\sim 40keV$ at $M \approx 9$ and recovers to $\sim 100keV$ at
 128 $M \approx 16$, indicating much softer electron spectra inside the whistler-mode slot region than
 129 in the whistler-mode belts.

130 The total energy flux ϵ_T of energetic electrons with differential flux $j(E)$ is calculated
 131 with

$$\epsilon_T = 4\pi \int_{E_{min}}^{E_{max}} j \cdot E dE. \quad (3)$$

132 The factor 4π is used for the omni-directional electron population measured near the
 133 magnetic equator. The dark blue curve and error bars in Figure 3(c) show the median
 134 value, lower and upper quartile of T as a function of M-shell. Sharp decreases in T are
 135 distinct at $M \approx 9$ and $M \approx 16$, the boundaries of electron slot region.

136 The colocation of the Jovian whistler-mode and energetic electrons slot regions is likely
 137 not a coincidence. Previous studies [Menietti *et al.*, 2021a, b] suggest that whistler-mode
 138 dynamics in Jovian inner and middle magnetosphere are controlled by the intensity of 100s
 139 keV electrons. The cyclotron resonance condition between electrons and whistler-mode
 140 waves can be expressed as

$$\omega - k_{\parallel}v_{\parallel} = n|\Omega_e|/\gamma, \quad (4)$$

141 where k_{\parallel} and v_{\parallel} are the field-aligned components of the wave propagation vector and
 142 particle velocity, ω and $\Omega_e = 2\pi f_{ce}$ are the angular frequency of the wave and electrons,

143 γ is the relativistic factor and $n = 0, \pm 1, \pm 2, \dots$ is an integer referred to as the order of
 144 cyclotron resonance.

145 Equation 4 is used to calculate the minimum resonant energy (MRE) for the first-order
 146 cyclotron resonance ($n = 1$) between electrons and whistler-mode waves, which mainly
 147 control the growth and damping rates of whistler-mode chorus waves along with the
 148 Landau resonance ($n = 0$) [Kennel and Petschek, 1966; Li et al., 2010]. A plasma density
 149 model from Galileo measurements [Frank et al., 2002] is used. The red curves in Figure
 150 3(c) show the MRE for electrons in the $n = 1$ cyclotron resonance with the $f = 0.1f_{ce}$ and
 151 $f = 0.5f_{ce}$ field-aligned whistler-mode waves, respectively. Our calculation shows that
 152 for the $n = 1$ MRE for electrons and whistler-mode waves in the equatorial lower band
 153 chorus frequency range at the magnetic equator (the chorus source region) occurs in the
 154 10s to 100s of keV range at $5 \sim 25R_J$. Such a minimum resonance energy is close to the
 155 estimated characteristic electron energy.

156 Panels (d) and (e) of Figure 3 present the statistical pitch angle distribution (PAD) of
 157 electrons with an energy of ~ 178.6 keV and ~ 334.0 keV, respectively. Color-coded maps
 158 show the median value of the pitch angle-resolved differential electron fluxes in each (M, α)
 159 grid ($\Delta M = 0.5, \Delta \alpha = 10^\circ$), where α denotes the local pitch angle. We note that above
 160 $M = 21$, where the outer whistler-mode belt peaks, the bidirectional PAD distributions
 161 dominate, in agreement with Galileo observations [Tomás et al., 2004; Mauk and Saur,
 162 2007] that a correlation between the PAD transition and the mapping of Jovian diffuse
 163 auroral emissions was indicated. Leakage of auroral hiss waves from the diffuse auroral
 164 zone may also contribute to the whistler-mode wave intensity in our statistics (detailed in

165 Section 3.2). *Saur et al.* [2018] developed a theory of wave-particle interactions between
166 kinetic Alfvén waves (KAWs) and electrons in the Jovian magnetosphere, suggesting that
167 KAWs are capable of generating broadband bidirectional auroral electron beams. Further
168 investigation of the relationship among whistler-mode waves, bidirectional electron beams,
169 and KAWs is needed to reveal the mechanism of the outer-belt whistler-mode excitation
170 and the Jovian diffuse-aurora emission.

3.2. Local-time and Latitudinal Distribution of the Outer Whistler-mode Belt

171 As shown in Figure 2, the Juno extended mission reveals a stronger outer whistler-mode
172 belt measured in the dusk-premidnight sector than in the postmidnight-dawn sector. As
173 it took more than 6 years for Juno to scan from MLT0600 to MLT1800, such a variation
174 of wave intensity could either result from a temporal variation or a spatial asymmetry. In
175 this section, both scenarios will be examined.

176 The top panel of the supporting information Figure S3 presents the solar wind speed
177 and Lyman-alpha intensity during the time interval of the Juno orbit PJ01-PJ45. For the
178 first 45 orbits around Jupiter, Juno experienced both the descending phase of Solar Cycle
179 24 and the ascending phase of Solar Cycle 25. More high-speed solar wind events were
180 recorded during the descending phase of Solar Cycle 24 than during the ascending phase
181 of Solar Cycle 25. In contrast, the integrated chorus wave power measured in the outer
182 whistler-mode belt ($18 < M < 25$) increased almost monotonically from $6 \times 10^{-6} nT^2$
183 to $7 \times 10^{-6} nT^2$ (see the bottom panel of Figure S3). Therefore, the long-term intensity
184 variation of the outer whistler-mode belt is not positively correlated with the solar cycles.

185 The observed intensity variation is more likely to be an inherent dawn-dusk asymmetry
186 in the Jovian magnetosphere.

187 Figure 4 presents the intensity of the outer whistler-mode belt and the energetic electron
188 flux as a function of MLT. As the apogee of Juno precessed from the dawn to dusk, both the
189 integrated whistler-mode wave intensity and the energetic electron flux increased nearly
190 monotonically. Dusk intensities are around seven times stronger than at dawn. A similar
191 asymmetry trend is seen in energetic electrons (panel b). The energy spectrum measured
192 at dusk is also harder than at dawn. Since near-equatorial of 10s-100s keV electrons
193 are potential sources of outer-belt whistler-mode emissions (Section 3.1), we suggest that
194 such dawn-dusk asymmetries in both waves and energetic electrons spectra are likely
195 interconnected.

196 It is worth noting that in the analysis above the contribution of auroral hiss waves
197 cannot be fully eliminated [e.g., *Li et al.*, 2020; *Menietti et al.*, 2021b, 2023a]. Auroral
198 hiss has a source region in the auroral region and is observed by Juno at higher magnetic
199 latitudes and M-shells, and can be observed for large distances from its origin [*Gurnett*
200 *et al.*, 1983; *Sazhin et al.*, 1993]. *Menietti et al.* [2023a] set a limit on observations of
201 Jovian chorus emission at $|\lambda| < 31^\circ$ or $M < 20$. At a larger M-shell or higher magnetic
202 latitude, auroral hiss waves could become the dominant source of whistler-mode emission.
203 In Figure S4, we show an example of intense whistler-mode auroral hiss emission. This
204 is distinguished by the spectrogram wave morphology in the top two panels of Figure
205 S4, showing a generally smooth appearance with no distinct narrow band signature as
206 in the case of chorus. Chorus is known to have a source near the magnetic equator [cf.

207 *Hospodarsky et al.*, 2012]. The waves shown in Figure S4 propagate away from Jupiter
208 and toward the magnetic equator, which is consistent with auroral hiss. This is shown by
209 analyzing the phase of the waves relative to the E_y and B_z antennas of the Juno Waves
210 plasma wave instrument, as described in *Kolmašová et al.* [2018].

211 Distinguishing auroral hiss waves from chorus waves with the method shown above re-
212 quires burst-mode Juno Waves data, which are not always available for our study. Here
213 we attempt to identify the contribution of chorus and auroral hiss from the latitudinal
214 distribution of the wave intensity, shown Figure 2(b-c). For the inner whistler-mode
215 belt ($M < 12$), strong whistler-mode emissions concentrate in the near-equatorial region.
216 Therefore, the inner whistler-mode belt is more likely to be dominated by chorus waves.
217 For the outer-whistler belt, in the midnight-dawn sector there is also a peak of near-
218 equatorial wave intensity ($|\lambda| < 8^\circ$), indicating a possible contribution of chorus waves
219 generated near the magnetic equator. In the dusk-midnight sector, the latitudinal depen-
220 dence in mean wave intensity is not clear. In Figure 4(c), we further present the median
221 value of wave intensity in the outer whistler-mode belt. In midnight-dawn sector, the me-
222 dian value also shows a peak within $|\lambda| < 16^\circ$, which is most likely to be near-equatorial
223 chorus waves rather than auroral hiss waves. At $|\lambda| \approx 23.5^\circ$, another peak of the median
224 wave intensity appears, indicating the contribution of auroral hiss waves. In the dusk-pre-
225 midnight sector, the median wave intensity increases with $|\lambda|$ in the region $0^\circ \leq |\lambda| < 16^\circ$
226 and drops dramatically at $|\lambda| \approx 18.5^\circ$. We note that for the $|\lambda| > 16^\circ$ region, the orbital
227 coverage of Juno was limited in the dusk-midnight sector. Therefore, it is hard to de-
228 rive a complete latitudinal dependence of the wave intensity in the dusk-midnight sector

229 from the Juno measurements. Based on our analysis above, we suggest that the “outer
 230 whistler-mode belt” may consist of equatorial chorus waves and auroral hiss waves from
 231 the Jovian polar region. Orbit-by-orbit analysis of wave properties is needed to further
 232 reveal the physical nature of the intense wave emission at $18 < M < 25$.

4. Summary and Discussion

233 Using by the Juno spacecraft during its primary and extended mission, we resolve several
 234 concurrent features in whistler wave and energetic electron intensities:

- 235 1. There is a double-belt structure in the intensity of Jovian whistler-mode waves
 236 ($0.1f_{ceq} < f < 0.8f_{ceq}$) between $M=5$ and 25. An outer whistler-mode belt peaks at
 237 $M \approx 21$ and shows wave intensity comparable to an inner whistler-mode belt at $M < 9$.
- 238 2. Between the aforementioned whistler-mode belts, a “slot” region of low energetic
 239 electron fluxes is revealed. At the region where $9 < M < 16$ and $|\lambda| < 4^\circ$, the median
 240 fluxes of 100-700 keV electrons drop by over 2 orders of magnitude compared to the
 241 ambient environment. At $M \approx 21$, where the outer whistler-mode belt peaks, the pancake
 242 pitch angle distribution of 100 keV electrons switches to a bidirectional distribution.
- 243 3. The intensity of waves observed in the dusk-midnight sector of the outer whistler-
 244 mode belt is significantly higher than in the midnight-dawn sector. Fluxes of energetic
 245 electrons show a similar trend. Such distributions are most likely due to an inherent
 246 dawn-dusk asymmetry of the Jovian magnetosphere.
- 247 4. According to the latitudinal dependence of the wave intensity, the outer whistler-
 248 mode belt is a mixture of near-equatorial chorus waves and auroral hiss.

249 Since this study focused on the frequency range above $0.1f_{ceq}$, it is no surprise that the
250 spatial distribution patterns of wave intensity differ from previous studies starting from
251 the local proton frequency (f_{cp}) or the lower hybrid frequency (f_{lh}), with which waves of
252 lower frequency are counted [*Li et al.*, 2020; *Menietti et al.*, 2021a, b].

253 Juno observations have shown that the global distribution patterns of whistler-mode
254 waves and 100s of keV electrons share mutual features in both the radial and azimuthal
255 dimensions. Estimation of the minimum resonant energy for the $n = 1$ cyclotron resonance
256 indicates that the aforementioned electron population is likely to be the source electrons
257 that excite the whistler-mode waves. Given that such a peculiar global distribution pat-
258 tern of waves could be fully explained by the observed electron distribution pattern, the
259 mechanism that forms such an electron distribution map still remains enigmatic. Some
260 possible explanations are briefly discussed below.

261 Radial diffusion process alone cannot account for the presence of the electron slot. Losses
262 (absorption, scattering), and/or local acceleration are needed. Wave-particle interactions
263 at higher latitude (e.g., inside the auroral zone [*Saur et al.*, 2018; *Elliott et al.*, 2018]) or
264 from different frequency ranges than studied here (e.g., higher frequency Z-mode waves
265 [*Menietti et al.*, 2021b] or lower frequency EMIC/hiss waves [*Li et al.*, 2020]) may be
266 responsible. Comprehensive Fokker-Planck simulations considering realistic wave species
267 and distribution [e.g., *Nénon et al.*, 2017] may help to understand the role of wave-particle
268 interactions in the formation of the electron slot found in this study. We also highlight
269 that the inner and outer edges of the electron slot are located at $M \approx 9$ and $M \approx 16$,
270 which coincide with the orbits of Europa and Ganymede. Both satellites produce intense

271 whistler-mode wave emissions [*Shprits et al.*, 2018; *Kurth et al.*, 2022]. These localized
272 but very strong wave sources can drive local electron acceleration or loss [*Shprits et al.*,
273 2018; *Li et al.*, 2023].

274 Regarding the dawn-dusk electron flux asymmetry, several sources may account for
275 them [*Palmaerts et al.*, 2017, and references therein]. The brightness of the Io torus has a
276 significant dawn-dusk asymmetry [*Schneider and Trauger*, 1995; *Murakami et al.*, 2016],
277 which is believed to be driven by the dawn-to-dusk electric field [*Barbosa and Kivelson*,
278 1983; *Ip and Goertz*, 1983]. Such a dawn-to-dusk electric field has also recently been
279 utilized to explain the prompt acceleration of multi-MeV electrons at $M > 14R_J$ [*Rous-*
280 *sos et al.*, 2018; *Hao et al.*, 2020; *Yuan et al.*, 2021]. We suggest that the dawn-to-dusk
281 electric field may also explain the higher flux and harder energy spectra observed by both
282 Juno/JEDI (this study) and Galileo/EPD [*Yuan et al.*, 2024] at dusk in comparison to
283 the dawn flank. Another possible mechanism could be related to the corotation break-
284 down. Previous studies on ion flow anisotropies [*Krupp et al.*, 2001; *Waldrop et al.*, 2015]
285 indicated that the corotation of the Jovian plasma starts to breakdown at $15 \sim 20R_J$
286 in the dusk sector while remaining rigid or even super-corotational in the dawn sector.
287 Corotation breakdown may supply the heating and increase in the anisotropy of energetic
288 electrons and hence lead to stronger chorus wave emissions in the dusk magnetosphere.
289 Theoretical studies [*Kivelson and Southwood*, 2005; *Vogt et al.*, 2014] also discussed how
290 centrifugal forces contribute to particle anisotropy and their local time asymmetry during
291 outward expansion of flux tubes, which might also be related to dawn-dusk asymmetries
292 in energetic electron distributions reported in this study.

293 Finally, the possibility that long-term temporal variations resulted in the observed in-
294 homogeneity of the outer whistler-mode belt cannot be completely ruled out, as it took
295 6.1 years for Juno to achieve the map shown in Figure 2(a), approximately half of the
296 orbital period of Jupiter (11.86 years). Although in Section 3.2 we have shown that the
297 intensity of the outer whistler-mode belt is not likely to be positively correlated with solar
298 activity, the seasonal effect remains a potential explanation for the observed variations
299 in the Juno data. The strength of the coupling between the solar activity and the in-
300 ner magnetosphere of Jupiter remains an open question. Furthermore, due to the lack
301 of Juno equatorial coverage at MLT0000-0600 and $M < 12$, only the asymmetry of the
302 outer whistler-mode belt is discussed in the present study. Combining Galileo data [e.g.,
303 *Menietti et al.*, 2012; *Shprits et al.*, 2018; *Li et al.*, 2020] with Juno data may help to draw
304 a more conclusive picture of the whistler-mode wave distribution and temporal variation
305 after undergoing the necessary cross-calibrations.

5. Acknowledgement

306 Y. Y. S, J. D. M and T. F. A are supported by the NASA Survey of Jovian Plasma
307 Wave Intensity and Diffusive Modeling of Electron Acceleration and Scattering of Juno
308 Participating Scientist Program (80NSSC19K1262). Y. Y. S declares potential conflict
309 of interest and significant financial interest in Space Sciences Innovations Inc. in Seattle,
310 WA. The authors sincerely acknowledge Margaret G. Kivelson and Xianzhe Jia for the
311 discussion section.

6. Data Availability Statement

312 Juno JEDI data can be obtained at [https://pds-ppi.igpp.ucla.edu/search/](https://pds-ppi.igpp.ucla.edu/search/view/?f=yes&id=pds://PPI/JNO-J-JED-3-CDR-V1.0)
313 [view/?f=yes&id=pds://PPI/JNO-J-JED-3-CDR-V1.0](https://pds-ppi.igpp.ucla.edu/search/view/?f=yes&id=pds://PPI/JNO-J-JED-3-CDR-V1.0). Juno WAV data can be
314 obtained at [https://pds-ppi.igpp.ucla.edu/search/view/?f=yes&id=pds://PPI/](https://pds-ppi.igpp.ucla.edu/search/view/?f=yes&id=pds://PPI/JNO-E_J_SS-WAV-3-CDR-SRVFULL-V2.0)
315 [JNO-E_J_SS-WAV-3-CDR-SRVFULL-V2.0](https://pds-ppi.igpp.ucla.edu/search/view/?f=yes&id=pds://PPI/JNO-E_J_SS-WAV-3-CDR-SRVFULL-V2.0). Solar wind speed data can be obtained at
316 https://cdaweb.gsfc.nasa.gov/sp_phys/data/omni/hro_1min/. Solar Lyman-alpha
317 intensity data can be obtained at [https://cdaweb.gsfc.nasa.gov/sp_phys/data/](https://cdaweb.gsfc.nasa.gov/sp_phys/data/omni/hro_1min/)
318 [omni/hro_1min/](https://cdaweb.gsfc.nasa.gov/sp_phys/data/omni/hro_1min/)

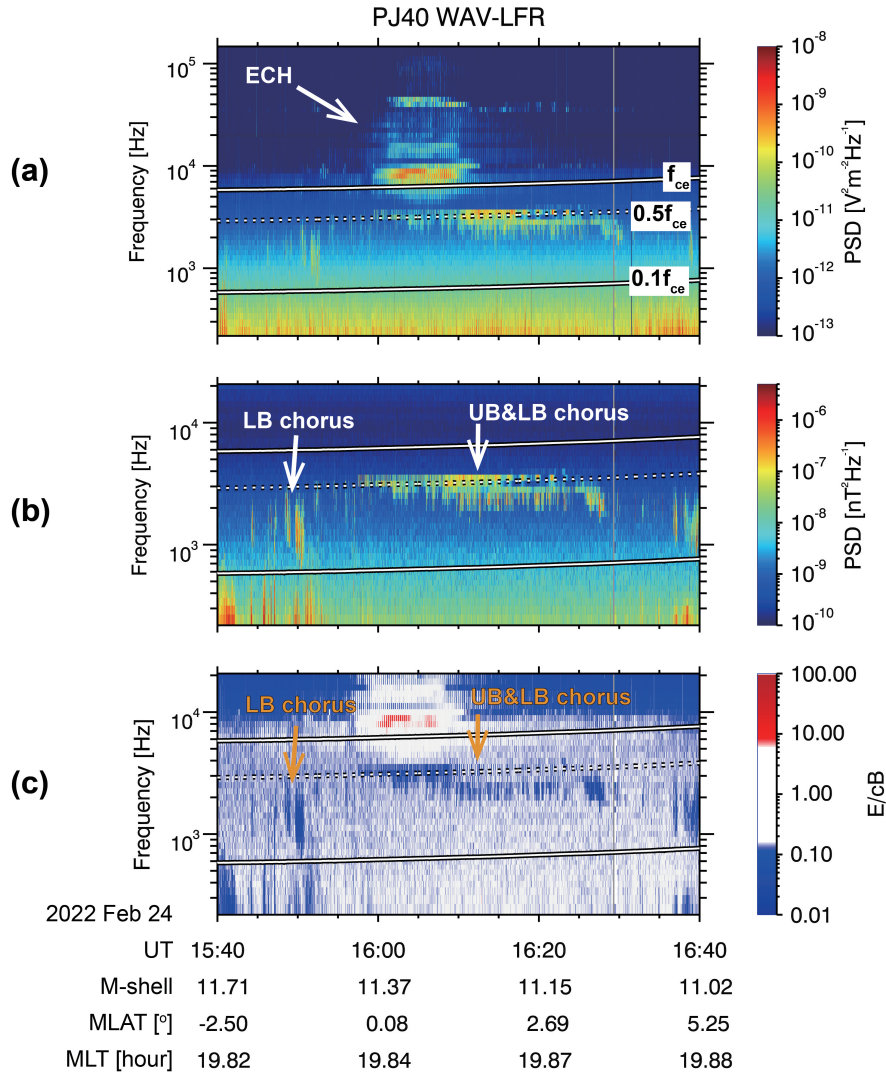


Figure 1. An example of whistler mode chorus waves observed by Juno near the magnetic equator of Jupiter. **(a)** Wave electrical power spectral density (PSD), **(b)** Wave magnetic PSD, **(c)** E/cB during a magnetic equator passage of Juno's PJ40 orbit, showing ECH waves, lower-band (LB) and upper-band (UB) chorus. White curves in each panel indicate local f_{ce} , $0.5f_{ce}$ and $0.1f_{ce}$ values.

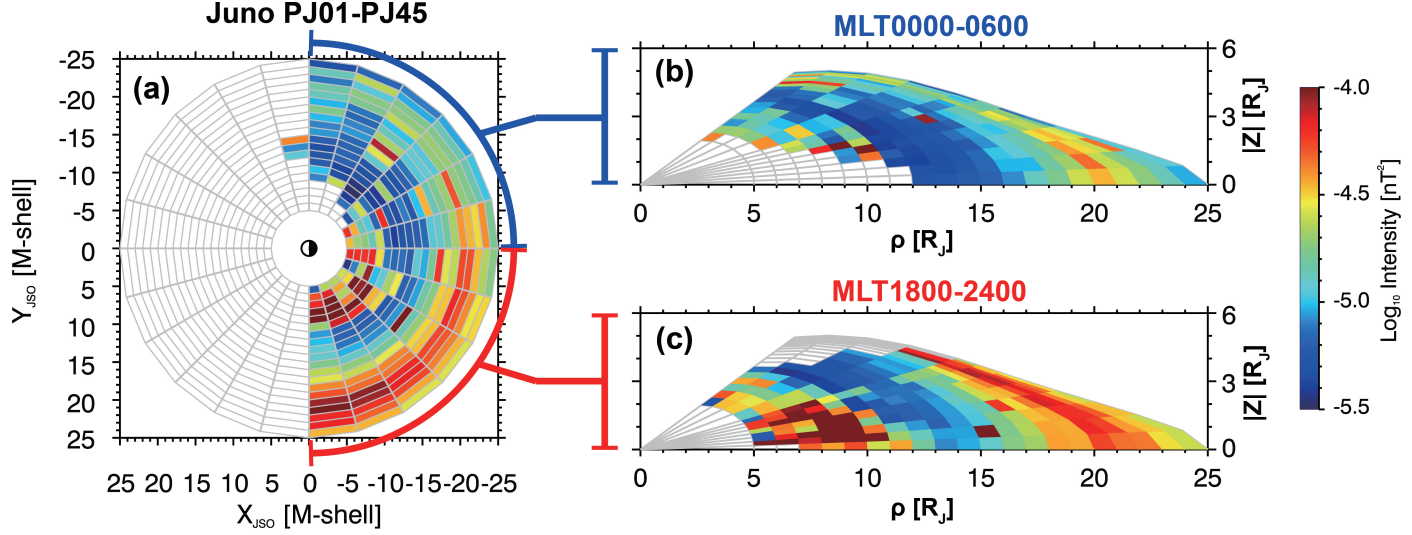


Figure 2. Whistler-mode wave intensity distribution. (a) M-shell versus MLT intensity spectrogram. (b, c) Wave intensity spectrogram in meridian plane for two MLT ranges. (c) Same format as panel (b) but for MLT from 1800 to 2400 (dusk-premidnight sector). Color coded are mean values of integrated wave intensity $\langle B_W^2 \rangle$ integrated between $0.1f_{ceq} < f < 0.8f_{ceq}$.

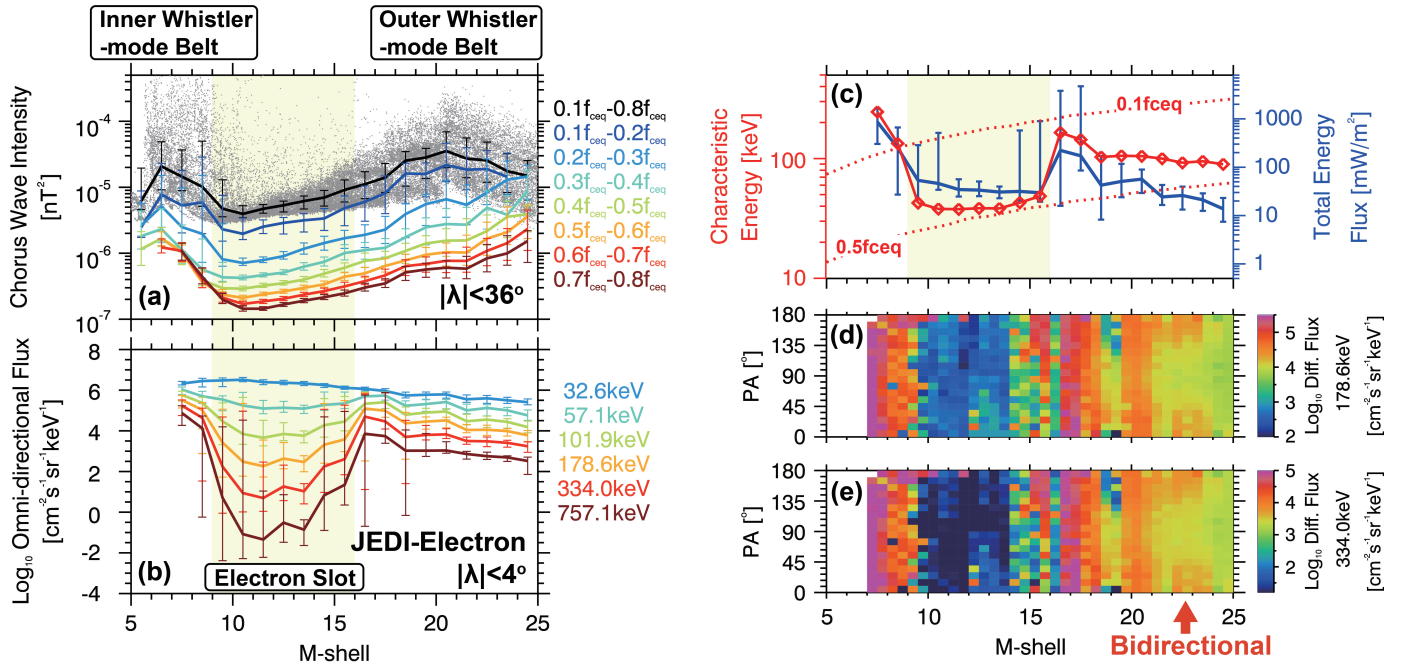


Figure 3. Statistical radial profile of whistler-mode waves and energetic electrons measured by Juno during orbits PJ01 through PJ45. **(a)** Whistler-mode wave intensity against M-shell. The gray points are 1-minute averaged wave intensities. Solid curves present median values of wave intensity in each frequency bin (colored) and total integrated wave intensity (black). **(b)** Median omni-directional electron differential fluxes against M-shell measured near the magnetic equator. **(c)** Characteristic energy and total energy flux derived from JEDI measurements. Dotted curves show the minimum energy for cyclotron resonance between electrons and whistler-mode waves with the frequencies $0.1f_{ceq}$ and $0.5f_{ceq}$. The energetic electron slot is marked with light yellow. **(d)-(e)** Median pitch angle distribution of $\sim 179\text{keV}$ and $\sim 334\text{keV}$ electrons.

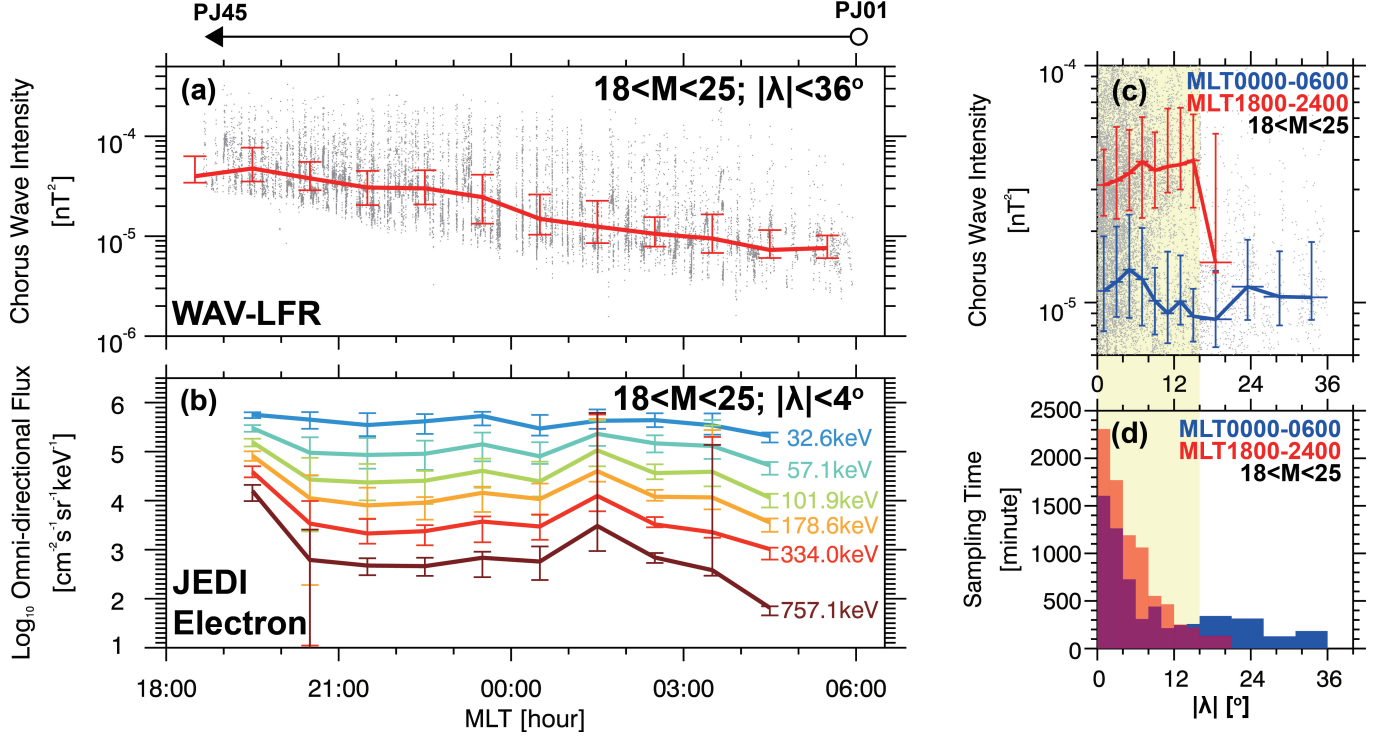


Figure 4. Local time asymmetry of the wave intensity and electron flux in the outer whistler-mode belt. (a) Whistler-mode wave intensity as a function of MLT. The solid curve shows the median wave intensity integrated from $0.1f_{ceq}$ to $0.8f_{ceq}$ within $18 < M < 25$ and $|\lambda| < 36^\circ$. Gray points show the scatter plot of 1-minute averaged, wave intensity integrated from $0.1f_{ceq}$ to $0.8f_{ceq}$. (b) Median, upper, and lower quartiles of omnidirectional electron fluxes as a function of the MLT measured near the magnetic equator. (c) Integrated wave intensity as a function of $|\lambda|$. Blue (red) curve denotes the median wave intensity sampled in the midnight-dawn (dusk-midnight) sector. Gray points are the same data as in panel (a) but plotted as against $|\lambda|$. (d) Sampling time as a function of $|\lambda|$ at $18 < M < 25$ in each MLT sector.

References

- Allison, H. J., Y. Y. Shprits, I. S. Zhelavskaya, D. Wang, and A. G. Smirnov, Gyroresonant wave-particle interactions with chorus waves during extreme depletions of plasma density in the van allen radiation belts, *Science Advances*, 7(5), eabc0380, 2021.
- Barbosa, D., and M. Kivelson, Dawn-dusk electric field asymmetry of the io plasma torus, *Geophysical Research Letters*, 10(3), 210–213, 1983.
- Burtis, W., and R. Helliwell, Banded chorus—a new type of vlf radiation observed in the magnetosphere by ogo 1 and ogo 3, *Journal of Geophysical Research*, 74(11), 3002–3010, 1969.
- Burton, R. K., and R. E. Holzer, The origin and propagation of chorus in the outer magnetosphere, *Journal of Geophysical Research*, 79(7), 1014–1023, 1974.
- Connerney, J., M. Acuna, and N. Ness, Modeling the jovian current sheet and inner magnetosphere, *Journal of Geophysical Research: Space Physics*, 86(A10), 8370–8384, 1981.
- Connerney, J., et al., The juno magnetic field investigation, *Space Science Reviews*, 213, 39–138, 2017.
- Connerney, J., et al., A new model of jupiter’s magnetic field from juno’s first nine orbits, *Geophysical Research Letters*, 45(6), 2590–2596, 2018.
- Elliott, S., D. Gurnett, W. Kurth, B. Mauk, R. Ebert, G. Clark, P. Valek, F. Allegrini, and S. Bolton, The acceleration of electrons to high energies over the jovian polar cap via whistler mode wave-particle interactions, *Journal of Geophysical Research: Space Physics*, 123(9), 7523–7533, 2018.
- Frank, L., W. Paterson, and K. Khurana, Observations of thermal plasmas in jupiter’s magnetotail, *Journal of Geophysical Research: Space Physics*, 107(A1), SIA–1, 2002.

- Gurnett, D., W. Kurth, A. Roux, S. Bolton, and C. Kennel, Evidence for a magnetosphere at ganymede from plasma-wave observations by the galileo spacecraft, *Nature*, 384(6609), 535–537, 1996.
- Gurnett, D. A., S. D. Shawhan, and R. R. Shaw, Auroral hiss, z mode radiation, and auroral kilometric radiation in the polar magnetosphere: De 1 observations, *Journal of Geophysical Research: Space Physics*, 88(A1), 329–340, 1983.
- Hao, Y.-X., et al., The formation of saturn’s and jupiter’s electron radiation belts by magnetospheric electric fields, *The Astrophysical Journal Letters*, 905(1), L10, 2020.
- Horne, R. B., R. M. Thorne, S. A. Glauert, J. Douglas Menietti, Y. Y. Shprits, and D. A. Gurnett, Gyro-resonant electron acceleration at jupiter, *Nature Physics*, 4(4), 301–304, 2008.
- Horne, R. B., et al., Wave acceleration of electrons in the van allen radiation belts, *Nature*, 437(7056), 227–230, 2005.
- Hospodarsky, G., K. Sigsbee, J. Leisner, J. Menietti, W. Kurth, D. Gurnett, C. Kletzing, and O. Santolík, Plasma wave observations at earth, jupiter, and saturn, *Dynamics of the Earth’s radiation belts and inner magnetosphere*, 199, 415–430, 2012.
- Ip, W.-H., and C. Goertz, An interpretation of the dawn–dusk asymmetry of uv emission from the io plasma torus, *Nature*, 302(5905), 232–233, 1983.
- Kennel, C. F., and H. E. Petschek, Limit on Stably Trapped Particle Fluxes, *J. Geophys. Res.*, , 71, 1–+, 1966.
- Kivelson, M., and D. Southwood, Dynamical consequences of two modes of centrifugal instability in jupiter’s outer magnetosphere, *Journal of Geophysical Research: Space Physics*, 110(A12), 2005.

- Kolmašová, I., M. Imai, O. Santolík, W. S. Kurth, G. B. Hospodarsky, D. A. Gurnett, J. E. Connerney, and S. J. Bolton, Discovery of rapid whistlers close to jupiter implying lightning rates similar to those on earth, *Nature Astronomy*, *2*(7), 544–548, 2018.
- Krupp, N., A. Lagg, S. Livi, B. Wilken, J. Woch, E. Roelof, and D. Williams, Global flows of energetic ions in jupiter’s equatorial plane: First-order approximation, *Journal of Geophysical Research: Space Physics*, *106*(A11), 26,017–26,032, 2001.
- Kurth, W., G. Hospodarsky, D. Kirchner, B. Mokrzycki, T. Averkamp, W. Robison, C. Piker, M. Sampl, and P. Zarka, The juno waves investigation, *Space Science Reviews*, *213*, 347–392, 2017.
- Kurth, W. S., et al., Juno plasma wave observations at ganymede, *Geophysical research letters*, *49*(23), e2022GL098,591, 2022.
- Lauben, D. S., U. S. Inan, T. F. Bell, and D. Gurnett, Source characteristics of elf/vlf chorus, *Journal of Geophysical Research: Space Physics*, *107*(A12), SMP–10, 2002.
- Li, W., Q. Ma, R. Thorne, J. Bortnik, C. Kletzing, W. Kurth, G. Hospodarsky, and Y. Nishimura, Statistical properties of plasmaspheric hiss derived from van allen probes data and their effects on radiation belt electron dynamics, *Journal of Geophysical Research: Space Physics*, *120*(5), 3393–3405, 2015.
- Li, W., X.-C. Shen, J. Menietti, Q. Ma, X.-J. Zhang, W. Kurth, and G. Hospodarsky, Global distribution of whistler mode waves in jovian inner magnetosphere, *Geophysical Research Letters*, *47*(15), e2020GL088,198, 2020.
- Li, W., et al., Themis analysis of observed equatorial electron distributions responsible for the chorus excitation, *Journal of Geophysical Research: Space Physics*, *115*(A6), 2010.

- Li, W., et al., Driver of energetic electron precipitation in the vicinity of ganymede, *Geophysical Research Letters*, 50(6), e2022GL101,555, 2023.
- Ma, Q., et al., Energetic electron distributions near the magnetic equator in the jovian plasma sheet and outer radiation belt using juno observations, *Geophysical Research Letters*, 48(24), e2021GL095,833, 2021.
- Mauk, B., and N. Fox, Electron radiation belts of the solar system, *Journal of Geophysical Research: Space Physics*, 115(A12), 2010.
- Mauk, B., D. Mitchell, R. McEntire, C. Paranicas, E. Roelof, D. Williams, S. Krimigis, and A. Lagg, Energetic ion characteristics and neutral gas interactions in jupiter's magnetosphere, *Journal of Geophysical Research: Space Physics*, 109(A9), 2004.
- Mauk, B., et al., The jupiter energetic particle detector instrument (jedi) investigation for the juno mission, *Space Science Reviews*, 213, 289–346, 2017.
- Mauk, B. H., and J. Saur, Equatorial electron beams and auroral structuring at jupiter, *Journal of Geophysical Research: Space Physics*, 112(A10), 2007.
- Menietti, J., Y. Shprits, R. Horne, E. Woodfield, G. Hospodarsky, and D. Gurnett, Chorus, ech, and z mode emissions observed at jupiter and saturn and possible electron acceleration, *Journal of Geophysical Research: Space Physics*, 117(A12), 2012.
- Menietti, J., T. Averkamp, M. Imai, W. Kurth, G. Clark, F. Allegrini, J. Groene, J. Faden, and S. Bolton, Low-latitude whistler-mode and higher-latitude z-mode emission at jupiter observed by juno, *Journal of Geophysical Research: Space Physics*, 126(2), e2020JA028,742, 2021a.
- Menietti, J., T. Averkamp, W. Kurth, J. Faden, and S. Bolton, Survey and analysis of whistler- and z-mode emission in the juno extended mission, *Journal of Geophysical Research: Space*

Physics, 128(12), e2023JA032,037, 2023a.

Menietti, J., P. Yoon, T. Averkamp, W. Kurth, J. Faden, F. Allegrini, P. Kollmann, and S. Bolton, Wave and particle analysis of z-mode and o-mode emission in the jovian inner magnetosphere, *Journal of Geophysical Research: Space Physics*, p. e2022JA031199, 2023b.

Menietti, J., et al., Analysis of whistler-mode and z-mode emission in the juno primary mission, *Journal of Geophysical Research: Space Physics*, 126(11), e2021JA029,885, 2021b.

Meredith, N. P., R. B. Horne, A. Sicard-Piet, D. Boscher, K. H. Yearby, W. Li, and R. M. Thorne, Global model of lower band and upper band chorus from multiple satellite observations, *Journal of Geophysical Research: Space Physics*, 117(A10), 2012.

Murakami, G., et al., Response of jupiter's inner magnetosphere to the solar wind derived from extreme ultraviolet monitoring of the io plasma torus, *Geophysical Research Letters*, 43(24), 12–308, 2016.

Nénon, Q., A. Sicard, and S. Bourdarie, A new physical model of the electron radiation belts of jupiter inside europa's orbit, *Journal of Geophysical Research: Space Physics*, 122(5), 5148–5167, 2017.

Palmaerts, B., M. F. Vogt, N. Krupp, D. Grodent, and B. Bonfond, Dawn-dusk asymmetries in jupiter's magnetosphere, *Dawn-dusk asymmetries in planetary plasma environments*, pp. 307–322, 2017.

Roussos, E., P. Kollmann, N. Krupp, C. Paranicas, K. Dialynas, N. Sergis, D. Mitchell, D. Hamilton, and S. Krimigis, Drift-resonant, relativistic electron acceleration at the outer planets: Insights from the response of saturn's radiation belts to magnetospheric storms, *Icarus*, 305, 160–173, 2018.

- Saur, J., et al., Wave-particle interaction of alfvén waves in jupiter’s magnetosphere: Auroral and magnetospheric particle acceleration, *Journal of Geophysical Research: Space Physics*, *123*(11), 9560–9573, 2018.
- Sazhin, S., K. Bullough, and M. Hayakawa, Auroral hiss: A review, *Planetary and space science*, *41*(2), 153–166, 1993.
- Schneider, N. M., and J. T. Trauger, The structure of the io torus, *The Astrophysical Journal*, *450*, 450, 1995.
- Shprits, Y., J. Menietti, X. Gu, K.-C. Kim, and R. Horne, Gyroresonant interactions between the radiation belt electrons and whistler mode chorus waves in the radiation environments of earth, jupiter, and saturn: A comparative study, *Journal of Geophysical Research: Space Physics*, *117*(A11), 2012.
- Shprits, Y. Y., et al., Strong whistler mode waves observed in the vicinity of jupiter’s moons, *Nature communications*, *9*(1), 3131, 2018.
- Teng, S., X. Tao, and W. Li, Typical characteristics of whistler mode waves categorized by their spectral properties using van allen probes observations, *Geophysical Research Letters*, *46*(7), 3607–3614, 2019.
- Tomás, A. T., J. Woch, N. Krupp, A. Lagg, K.-H. Glassmeier, and W. S. Kurth, Energetic electrons in the inner part of the jovian magnetosphere and their relation to auroral emissions, *Journal of Geophysical Research: Space Physics*, *109*(A6), 2004.
- Tsurutani, B. T., and E. J. Smith, Postmidnight chorus: A substorm phenomenon, *Journal of Geophysical Research*, *79*(1), 118–127, 1974.

- Tsurutani, B. T., and E. J. Smith, Two types of magnetospheric elf chorus and their substorm dependences, *Journal of Geophysical Research*, 82(32), 5112–5128, 1977.
- Vogt, M. F., M. G. Kivelson, K. K. Khurana, R. J. Walker, M. Ashour-Abdalla, and E. J. Bunce, Simulating the effect of centrifugal forces in jupiter’s magnetosphere, *Journal of Geophysical Research: Space Physics*, 119(3), 1925–1950, 2014.
- Waldrop, L., E. Roelof, and T. Fritz, Three-dimensional convective flows of energetic ions in jupiter’s equatorial magnetosphere, *Journal of Geophysical Research: Space Physics*, 120(12), 10–506, 2015.
- Wang, D., Y. Y. Shprits, I. S. Zhelavskaya, O. V. Agapitov, A. Y. Drozdov, and N. A. Aseev, Analytical chorus wave model derived from van allen probe observations, *Journal of Geophysical Research: Space Physics*, 124(2), 1063–1084, 2019.
- Wang, J.-z., J.-n. Ma, Z.-x. Huo, Y. Xiong, and D. Tian, Statistical study of energetic electrons in jupiter’s inner magnetosphere by juno/jedi, *Advances in Space Research*, 67(5), 1709–1720, 2021.
- Woodfield, E. E., R. B. Horne, S. A. Glauert, J. D. Menietti, and Y. Shprits, The origin of jupiter’s outer radiation belt, *Journal of Geophysical Research: Space Physics*, 119(5), 3490–3502, 2014.
- Yuan, C., Y. Zuo, E. Roussos, Y. Wei, Y. Hao, Y. Sun, and N. Krupp, Large-scale episodic enhancements of relativistic electron intensities in jupiter’s radiation belt, *Earth and Planetary Physics*, 5(4), 314–326, 2021.
- Yuan, C., E. Roussos, Y. Wei, N. Krupp, Z. Liu, and J. Wang, Galileo observation of electron spectra dawn-dusk asymmetry in the middle jovian magnetosphere: Evidence for convection

electric field, *Geophysical Research Letters*, 51(1), e2023GL105,503, 2024.

Zhao, H., et al., Plasmaspheric hiss waves generate a reversed energy spectrum of radiation belt electrons, *Nature Physics*, 15(4), 367–372, 2019.